Chinese Journal of Aeronautics, (2014),27(2): 453–460

Chinese Society of Aeronautics and Astronautics
& Beihang University

Chinese Journal of Aeronautics

cja@buaa.edu.cn
www.sciencedirect.com

A fuzzy PID-controlled SMA actuator for a two-DOF joint

Shi Zhenyun, Wang Tianmiao, Liu Da *, Ma Chen, Yuan Xiangnan

Robotic Laboratory, Beihang University, Beijing 100191, China

Received 7 April 2013; revised 29 April 2013; accepted 30 May 2013
Available online 28 February 2014

KEYWORDS

Fuzzy PID control;
Mechanical Joint;
Self-sensing;
Shape memory alloy;
Smart structure

Abstract Shape memory alloy (SMA) actuator is a potential advanced component for servo-systems of aerospace vehicles and aircraft. This paper presents a joint with two degrees of freedom (DOF) and a mobility range close to ±60° when driven by SMA triple wires. The fuzzy proportional-integral-derivative (PID)-controlled actuator drive was designed using antagonistic SMA triple wires, and the resistance feedback signal made a closed loop. Experiments showed that, with the driving responding frequency increasing, the overstress became harder to be avoided at the position under the maximum friction force. Furthermore, the hysteresis gap between the heating and cooling paths of the strain-to-resistance curve expanded under this condition. A fuzzy logic control was considered as a solution, and the curves of the wires were then modeled by fitting polynomials so that the measured resistance was used directly to determine the control signal. Accurate control was demonstrated through the step response, and the experimental results showed that under the fuzzy PID-control program, the mean absolute error (MAE) of the rotation angle was about 3.147°. In addition, the investigation of the external interference to the system proved the controllable maximum output.

1. Introduction

Shape memory alloy (SMA) is a metal that exhibits a crystal transition up to or below a critical temperature that causes it alternate between the austenite phase and the martensite phase. In the martensite phase, SMA is soft and has inelastic straining[1]; however, in the austenite phase, the structure can contract back to its original shape, with an elastic modulus of roughly 100 GPa. Moreover, the maximum recoverable strain is more than 5% of the original length, even under some obstructions. With the growing demands for miniature applications, SMA actuators have been used in miniature mechanical devices due to their simple designs and high power-to-weight ratios.

In aerospace systems, SMA actuators can be developed as important components for future space vehicles and aircraft. For space vehicles, SMA actuators can be applied in advanced servo-systems, such as thrust vector adjusting systems for satellite attitude control and manipulators of manned or unmanned space vehicles. Recently, a prototype SMA actuated locking device was developed for satellites.[2] In another hand, SMA actuators also show their potential to be applied in aircraft, such as servo-systems of smart aircraft to change aerodynamic shapes[3] and controlling systems of rudders of missiles. The Boeing Company applied for a patent which

* Corresponding author. Tel.: +86 10 82339507.
E-mail addresses: shichong1983623@hotmail.com (Z. Shi), drliuda@aliyun.com (D. Liu).

Peer review under responsibility of Editorial Committee of CJA.

ELSEVIER Production and hosting by Elsevier

1000-9361 © 2014 Production and hosting by Elsevier Ltd. on behalf of CSAA & BUAA. Open access under CC BY-NC-ND license.
http://dx.doi.org/10.1016/j.cja.2014.02.015

focused on several aircraft systems with SMA actuators in 2009, and the new actuator was used to couple a deployable device to the airfoil in different methods.[4] Another effort of SMA actuators has been to develop smart rotors for helicopters to minimize the problems of noise and vibration.[5]

Following the above applications, SMA actuators show their advantage for minimized structures in limited space. For better compactness, employment of self-sensing is required to reduce the amount of additional sensors. This would also increase the robustness and fail-safety of the system. As a smart material, the electrical resistance of an SMA undergoes an observable change with a metallographic transformation, which is much more noticeable than the resistance change due to the metal's shape. Many studies have described the relationship between the strain and the resistance of an SMA, but the associated mathematical modeling is completely different when the components of the SMA change.[6] Moreover, in addition to temperature, stress can also affect the on-time electric resistance value of an SMA.[7]

Many groups[6,8–13] have developed actuators that use resistance as a sensor, and most of these studies focused on wire-spring actuators. Since the driving unit is inactive, achieving sufficient simultaneous stiffness and compactness with a spring is difficult. Compared with conventional SMA devices that require bias force components, antagonistic SMA multi-wire actuators with self-sensing capabilities show fully reversible responses,[7] and also have a higher response frequency, which shows their potential for wide applications. Based on antagonistic SMA multi-wire actuators, some instruments have been designed for applications,[14–17] although the nonlinear stiffness of the SMA wires during phase transformation offers a complex inner stress between antagonistic SMA wires, especially when the structure is complex. As shown in Fig. 1, the joint uses three SMA wires to achieve two degrees of freedom (DOF), which show an indeterminate amount of inner stress under different postures. The inner stress varies with the phase transformation of SMA wires and the friction force between the discs and the ball link of the joint.

The nonlinear inner stress requires the construction of self-sensing models with a variable coefficient, which is quite difficult to achieve. Furthermore, a way of knowing all inner-stress characteristics is needed. However, in real-world applications, measurements of inner stress are unachievable, due to the demand for compact devices. Nevertheless, a "black box" control method can accomplish the task.

As with many other smart materials, the hysteresis properties of SMA actuators show significant impact on the accuracy and stability in a regulation. To overcome the hysteresis properties of SMA actuators, researchers often choose a combination of a feedforward controller and a feedback loop. Specifically, the Preisach model,[12,18] neural network,[8] and Duhem differential[19] have been used to model hysteresis properties. Another possible solution is an SMA wire resistance controller,[20] in which the feedback signal is the simple linearized law between the wire strain and resistance values, assuming a sufficient load. A nonlinear proportional-integral-derivative (PID) controller is an option to improve the stability of the system and simultaneously reduce energy consumption.[21–23] Most of the aforementioned platforms perform under linear stress with less interference. Further research on the use of an antagonistic pair of SMA wires in an actuator with nonlinear stress has shown improved accuracy by limiting inner stress to a narrow range.[24] Yet, this is harder to achieve within more complicated structures, as shown in Fig. 1. Fuzzy logic control is another way to construct the controller with resistance feedback under nonlinear inner stress,[25,26] which is particularly well suited for uncertain or nonlinear conditions.

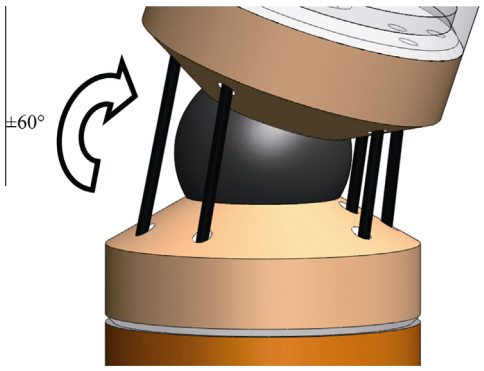

Fig. 1 Envisioned function of the end effector.

In this paper, we present our research on fuzzy PID-controlled architectures for an actuator with antagonistic SMA multi-wires, a newly designed two-DOF joint, and a resistance feedback signal that makes a closed loop. Consequently, a new approach for precision is proposed, which is sensorless SMA servo control: the hysteresis paths of both wires are modeled using polynomial functions and a fuzzy PID controller is used to reduce the overstress and improve the responding speed. In Section 2, the experimental setup of the testing platforms is described. After the basic kinematic model is described in Section 3, the internal force disturbing of the strain-to-resistance (S–R) curve is analyzed, and the modeling of the SMA actuator and the control strategy of the actuator with three SMA wires are presented. The control scheme based on the fuzzy PID controller and the self-feedback model is presented in Section 4, and the experimental results are discussed. In Section 5, the conclusions drawn from this study are presented.

2. Experimental setup

To study the S–R hysteresis curves and the internal force of all SMA wires, a platform with three load cells was set up and combined with a two-DOF joint, 8 mm in diameter, as shown in Fig. 2. The end effector was held in the middle, and the three load cells were set up symmetrically under the actuator's bottom to confirm the on-time internal force. Three pairs of V-shaped, 470-mm-long, TiNi-based, Flexinol-LT SMA wires, measuring 0.381 mm in diameter, were assembled inside the actuator, which was connected to the load cells through the axis to prevent friction from affecting the test results when the angle was adjusted. The mechanism details of the SMA actuator are described in Section 3.

An electric circuit was constructed, as shown in Fig. 3. A multifunction data acquisition card (±10 V full-scale range, 18-bit resolution; PCI-6284, NI) was used to send the pulse width modulation (PWM) signal via the digital output and to measure V_R (the voltage across the external resistor) and V_{SMA} (the actual voltages across the SMA wire) via the analog input. A Darlington driver was used as a switching element to control the heating or cooling state of the SMA actuator. An

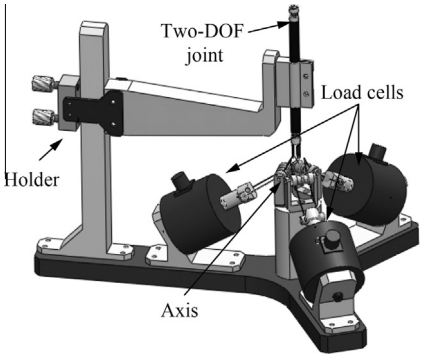

Fig. 2 Platform for triple-wire actuator.

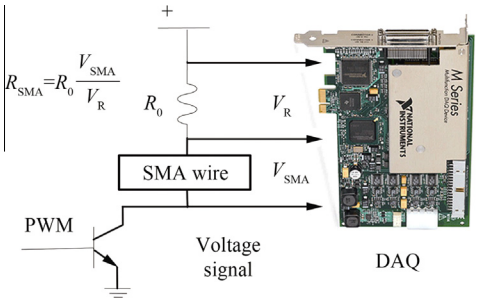

Fig. 3 Schematic of electric circuit.

external resistor (R_0), which was connected serially to the SMA actuator, was used as the standard resistance to measure the resistance value of the SMA wires (R_{SMA}).

3. Principle of antagonistic SMA triple-wire actuator

3.1. Structure of antagonistic SMA triple-wire actuator

To orient a system in all directions with a compact volume, a ball-joint link, as shown in Fig. 1, was an interesting solution. This structure showed good volume expenditure and potentially sufficient output.

In our design, the driving force from the SMA wires replaced traditional motors, which made the whole instrument more compact. As shown in Fig. 1, the architecture of the joint was composed of two discs and one spheroid. Through the holes in the two discs, four SMA wires (three for the ball-joint link and one for the grip) were set to supply the driving force. To maintain the pre-strain, a screw unit was set at the end of the wires to provide pre-strain to the SMA wires. The ball-joint link rotated around X and Y axes, and the last one was blocked by the wires; hence, the entire instrument included two DOFs for the pitch and yaw of the wrist. As mentioned in Section 2, a platform for studying the antagonistic triple-wire SMA actuator was set up, and the instrument was combined with it, as shown in Fig. 2.

Further tests were carried out, focusing on the S–R hysteresis curve of the triple wires and the on-time internal force situation. A binocular camera was used to monitor the rotating angle of the ball joint, as shown in Fig. 4. With a kinematic model, the strain of each wire was calculated, and three sets of S–R data for the wires were obtained.

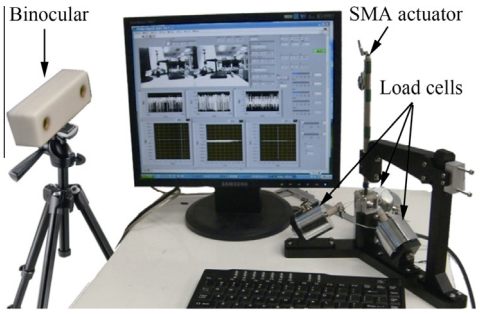

Fig. 4 Platform for triple-wire actuator monitor with a binocular camera.

The positions of the three controlling points (A, B, and C) were shifted by 120° relative to each other, with d representing the distance between the wires and the center of the discs. The ends of the three wires were placed on stationary points ($\boldsymbol{A}_0$, $\boldsymbol{B}_0$, and $\boldsymbol{C}_0$) on the bottom disc, which were $\Delta Z = -d$ when compared with the control points. If a rotation matrix is applied to these points, the universal rotational homogeneous transformation matrix $\boldsymbol{T}_i$ is given by

$$\boldsymbol{T}_i = \begin{bmatrix} \cos\alpha\cos\alpha\cos\beta+\sin\alpha\sin\alpha & \sin\alpha\cos\alpha\cos\beta-\sin\alpha\cos\alpha & -\sin\beta\cos\alpha \\ \sin\alpha\cos\alpha\cos\beta-\sin\alpha\cos\alpha & \sin\alpha\sin\alpha\cos\beta+\cos\alpha\cos\alpha & -\sin\alpha\sin\beta \\ \sin\beta\cos\alpha & \sin\alpha\sin\beta & \cos\beta \end{bmatrix} \tag{1}$$

where α and β define the desired orientation of the top disc with α representing the direction of the angulations with the X axis ($\pm 180°$) and β representing the direction with the Z axis ($\pm 60°$). These were chosen to set up the matrix to make the rotation position easier to view. Given the two desired angles, α and β, new points ($\boldsymbol{A}_i$, $\boldsymbol{B}_i$, and $\boldsymbol{C}_i$) were computed by multiplying $\boldsymbol{T}_i$ with the initial points. The difference between the controlling point, $\boldsymbol{A}_i$, and the stationary point, $\boldsymbol{A}_0$, is given by

$$\Delta S_A = |\boldsymbol{A}_i\boldsymbol{T}_i - \boldsymbol{A}_0| \tag{2}$$

where ΔS_A represents the strain of the SMA wires. Two marks were set up on the end effector and the arm so that the direction of the angulations could be observed with the deduced based on the displacements of the driving wires and the binocular camera. The S–R curve of every wire could be the tested resistance values.

3.2. S–R curve disturbed by internal force

Our previous studies of the S–R curve of the SMA wires proved that an appropriate pre-tension force could make the heating and cooling paths nearly overlap,[24] and it was simple to construct a polynomial model to apply the feedback control. Within the antagonistic pair of SMA wires actuator, enough pre-strain could also maintain enough inner stress between the wires, which minimized the hysteresis gap with the same principle.

Based on our previous study[24] of the pair of SMA wires actuator, it is concluded that the hysteresis gap between the heating and cooling curves is directly influenced by real-time internal force. With correct pre-strain, the hysteresis gap might be minimized. A polynomial model with one-to-one mapping was used to describe the S–R path of the SMA wires under convenient pre-strain.

The results presented in Section 3.1 were implemented in microcontroller language, which provided a solution for digital and analog commands. Firstly, the input pitch and roll angles were transformed into a target value of the wires' distance between the two discs, and the distance was treated as the target strain of the wires after being divided by the wires' original length. The binocular camera's data acquisition card collected the on-time rotation data of the end effector, which were transformed into the strain value of the three wires by Eq. (1) and Eq. (2). Before the resistance feedback module was constructed, visual feedback was used to achieve closed-loop control. The PWM drive signal of the three wires actuated the final disc, with a maximum of two wires being needed to serve as the driver at the same time, depending on the target posture. Three load cells collected the force information. The supply voltage was set at 12 V, and a pre-strain of 5% was applied before drive.

Thus, with enough pre-strain, the hysteresis gap between the heating and cooling paths of SMA wires should be minimized, although in the real application with the three-wire actuator, the gap appeared to be much wider near the middle of the strain position when overstressed. The *S*–*R* curve during overstress is shown in Fig. 5.

The internal force of SMA wires comes from two sources: the antagonistic force between driving and passive wires, and the friction force between the discs and the ball link, which varies with different joint postures, as shown in Fig. 6.

With zero posture, all the pressure from the wires applied to the top disc was transmitted to the ball link and transformed into friction force; with all the other postures, part of the pressure was assigned to the vertical direction, which made the friction force decrease when the rotation angle θ increased. The friction force is given by

$$f = \mu F \cos\theta \tag{3}$$

where f is the friction force between the discs and the ball link, μ is the friction factor, F indicates the pressure applied on the discs by the wires, and θ is the angle between the pressure and the axis. The varied friction force was difficult to test, but the internal force value of each wire was directly related to it and could be detected by the load cells. As shown in Fig. 7, the internal force scope of an SMA wire under different rotation angles, with respect to its vertical direction, was plotted, and the internal force boundary was scaled out. The internal force normally jumps to a higher value to reach another angle, and then drops to a lower stable plateau.

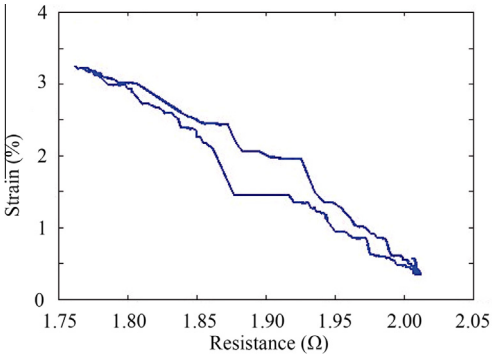

Fig. 5 *S*–*R* curve (wider hysteresis gap caused by overstress).

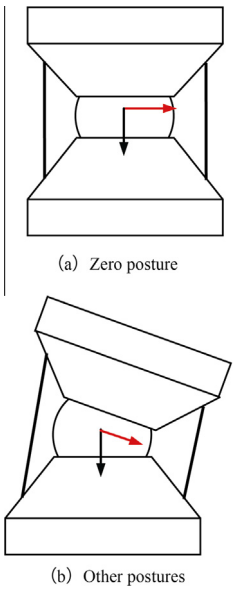

Fig. 6 Antagonistic force and friction force between discs and ball link.

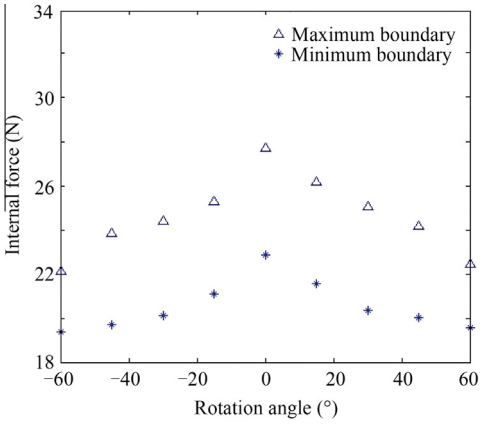

Fig. 7 Maximum and stabilized internal force of SMA wire under different rotation angles.

To minimize the hysteresis gap, a simple method is to reduce the heating speed to lessen the antagonistic force between driving and passive wires and eventually to decrease the pressure-related friction force. The improved *S*–*R* curve is shown in Fig. 8.

With a slower heating speed, the internal force scope of an SMA wire under different rotation angles with respect to its vertical direction is shown in Fig. 9. Although the stabilized internal force changed very little, the maximum internal force significantly dropped, indicating that the SMA wire could easily overcome stress during rotation.

Even though overstress can be solved simply with a reduction in heating speed, the responding frequency is limited under this condition. Fuzzy logic control simultaneously optimizes the frequency and internal force. By using the fuzzy controller, the majority of the cycle's responding speed can become faster, and overstress near the top position becomes limited. With fuzzy logic control, however, it is normally difficult

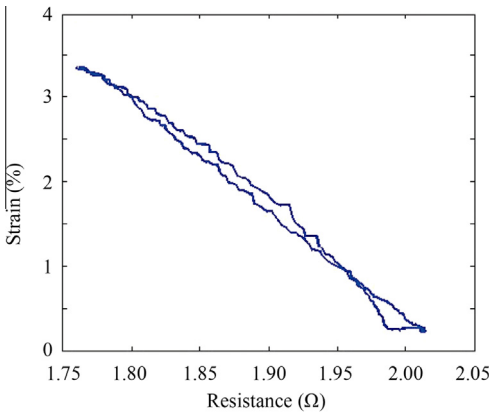

Fig. 8 *S–R* curve (under decreased inner stress).

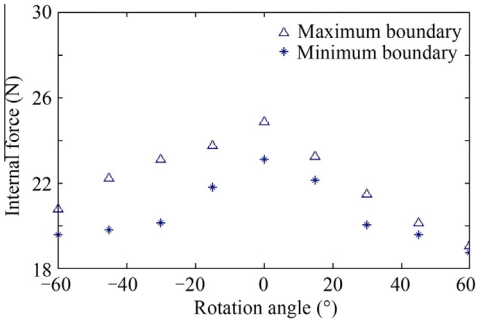

Fig. 9 Maximum and stabilized internal force of the SMA wire under different rotation angles with a slower heating speed.

to achieve accuracy — a requirement on the system. Nevertheless, a fuzzy PID control can maintain the flexible and adaptable fuzzy logic and supply accuracy with PID modules.

Before constructing the fuzzy PID controller, a necessary component of building a closed-loop control is the establishment of an *S–R* hysteresis model to convert the electric resistance value to the strain of the SMA wires. As noted by Lan and Fan[9] as well as in our previous work,[24] under convenient pre-strain, the heating and cooling paths are already quite close, and a polynomial model with one-to-one mapping is sufficient to describe the paths. In this experiment, the MATLAB "polyfit" function was used to obtain the coefficients of the polynomials. Tests verified that sixth-order polynomials had sufficient accuracy. Three V-shaped, 470-mm-long, TiNi-based, Flexinol-LT SMA wires, measuring 0.381 mm in diameter, were used. Two sixth-order polynomial fitting functions were then used to describe the *S–R* curve in Fig. 8 as follows:

$$R_h(S) = 0.0027S^6 + 0.0273S^5 - 0.1075S^4 + 0.2049S^3 - 0.1915S^2 - 0.0015S + 2.0207 \quad (4)$$

$$R_c(S) = 0.003S^6 - 0.0054S^5 + 0.0319S^4 - 0.0877S^3 + 0.1088S^2 - 0.1106S + 2.0154 \quad (5)$$

where R_c and R_h represent the resistance of the SMA wires, and subscripts "h" and "c" indicating the heating and cooling curves, respectively.

4. Fuzzy PID controller with self-sensing feedback

4.1. Control strategy

In developing the control, the SMA actuator was considered as a "black box." The input was the electric power supplied to the wires; the outputs were the joint posture and the generated force of every wire; the wire resistance was the internal variable.

The total power supplied can be represented by the product of $V_{SMA} \times I_{SMA} \times Dr$, I_{SMA} is the electric current through the SMA wire, and Dr is the duty ratio of heating. The dispersed power depends on material properties (specific heat) and environmental conditions (temperature and the coefficient of the convectional heat transfer), which is typically used to construct the feedforward compensator to eliminate overheating conditions. The feedforward compensator can be combined with the fuzzy PID control in the future, but that was not explored in this study.

The force generated by the SMA wires was measured by the load cells, which varied with the posture and helped to build the fuzzy logic to avoid overstress. The wire resistance was indirectly obtained via the setup shown in Fig. 3.

The input value of the controller is the desired strain (ε), and the self-sensing unit output is the corresponding resistance value, which is further converted to be the equivalent strain (ε^*). The difference between the two strain values is the positioning error, $e(n)$, which is subsequently multiplied by the proportional gain K_p. Its integral is multiplied by the integral gain K_i, and its derivative is amplified by means of the derivative gain K_d. The sum of these signals is the command duty ratio signal D_{out}, which is processed by the PWM to provide the electric heating. In the meantime, to reduce the friction force at specific postures, the restriction error, $f(n)$, is obtained by comparing the equivalent strain with a preset constant strain value.

Both errors were supplied to the fuzzy PID controller. The position-error and restriction-error variables of a fuzzy control were defined and split into four to five different levels using linguistic variables: negative big (NB), negative small (NS), zero (Z0), positive small (PS), and positive big (PB). The negative variable of the position error was integrated into P. The fuzzy subsystem was used to calibrate the K_p, K_i, and K_d parameters of the PID controller. The internal variable K_p was described by four linguistic variables: zero (Z0), low (L), medium (M), and high (H), while the three variables other than M were sufficient to describe K_i and K_d.

Fig. 10(a) shows the membership functions for the position-error variable. Since the actuator stroke is 4% of the wires' original length, the absolute value's maximum error is four. Triangular and trapezoidal membership functions were chosen to reduce computational costs. Trapezoidal wide PB operated when the error was big; Z0 and PS occurred with a small error; negative was under overshoot. Fig. 10(b) shows the membership functions for the restriction-error variable. The membership function range ($-60°$ to $+60°$) was the rotation range to the vertical axis of each wire.

Fig. 11 shows the membership functions for the three output variables. There were three narrow triangular and one trapezoidal membership functions with nearly no intersections for K_p, and two triangular and one trapezoidal functions for K_i

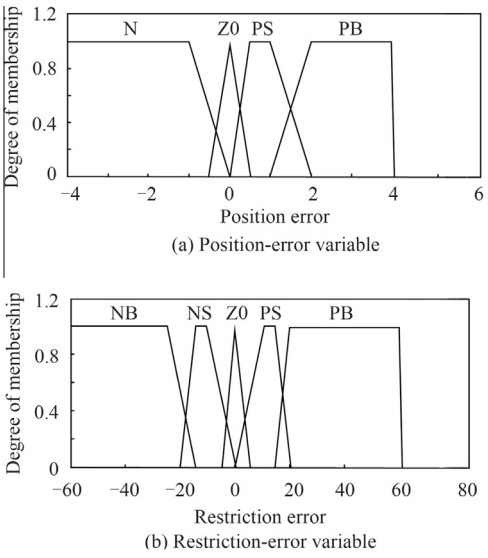

Fig. 10 Membership functions of position-error and restriction-error variables.

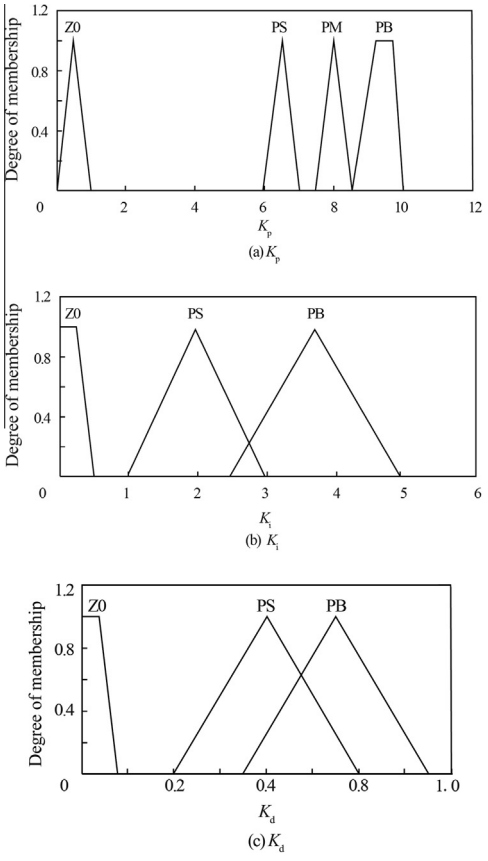

Fig. 11 Membership functions of output variables.

and K_d. The maximum heating speed was obtained with the 100% duty ratio, and the maximum cooling speed was achieved with zero input. The input voltage was 9.5 V, which could complete the phase transformation within 3 s under maximum duty ratio.

The rule set is composed as in Table 1.

As shown in Table 1, a negative (N) position error meant that the actuator overshot the desired strain, and the applied duty ratio was better when reduced to zero — considering that the cooling speed of the wires was very limited without extra cooling units. With the PB position error, higher proportion gain was necessary to speed up the responding frequency. The integral gain needed to increase when the position error reduced till zero to maintain stability, and the derivative gain needed to be chosen carefully to avoid vibration and to improve the responding frequency under different errors. Moreover, the absolute value of the restriction error indicates the distance between the equivalent position and the high friction point; the closer to the position, the lower the heating frequency has to be. These qualitative observations are the foundations of the inference rule set.

After using the polynomial model of Eqs. (4), (5) to obtain the feedback signal, the fuzzy PID controller was used to generate the duty cycle D_{out} of the PWM signal to implement the tracking. The expression of the appropriate duty cycle is

$$D(n) = K_p e(n) + K_i\{t_i[e(n) - e(n-1)] + S(n-1)\} + K_d[e(n) - e(n-1)] \quad (6)$$

where t_i is the sampling time. The parameters (K_p, K_i, and K_d) of the PID controller were auto-tuned by fuzzy logic rules. It is convenient to adopt the fuzzy reasoning method to determine the parameters based on the values of $e(n)$ and $f(n)$. Considering the symmetrical condition of the three wires, the same PID parameters were used for all three. Three groups of PWM signals were applied to the three wires separately during the control, and the wires carried out the duty of the drivers in turn. Fig. 12 shows the fuzzy PID control diagram.

4.2. Experimental results

To determine the accuracy of the proposed control scheme, various groups of tests were performed. The experiments used a multistep control signal, and the rotation boundary was tested in all directions. The boundary in β direction was $\pm 60°$, the same as the rotation angle around X and Y axes. In α direction, there was no obstacle for the whole cycle, from 0° to 360°.

To evaluate the accuracy of the response, Fig. 13 shows the rotation angles of β direction. The rotation angles remained constant at 30° in α direction and changed in β direction. The increment in each step was 15° over roughly 0.8 s; the desired angle and the actual angle showed visible constant error, which might be due to the difference between the control model and the real S–R curve. As indicated by the results, a maximum 3° overshoot appeared at the beginning of every step, and a feedforward compensator will be required in the future. The points were recorded every 0.04 s.

To study the difference between the desired angle and the actual angle rotation, the mean absolute error (MAE) of the multistep response was used to evaluate the accuracy of the models. The tracking MAE of the rotation angle was 3.147°. Furthermore, the internal force scopes of the SMA wires under different rotation angles were further narrowed, which proved the fuzzy logic theory.

To determine control accuracy under external interference (controllable maximum output), some further disturbance tests were done with the zero position during step responding

Table 1 Rule set of fuzzy PID controller.

Position error e	K_{PID}				
	f = NB	f = NS	f = Z0	f = PS	f = PB
PB	PB	PB	PM	PB	PB
	Z0	Z0	Z0	Z0	Z0
	PS	PS	PB	PS	PS
PS	PM	PM	PM	PM	PM
	PS	PS	PB	PS	PS
	PS	PS	PB	PS	PS
Z0	PM	PM	PM	PM	PM
	PB	PB	PB	PB	PB
	Z0	Z0	PS	Z0	Z0
N	Z0	Z0	Z0	Z0	Z0
	Z0	Z0	Z0	Z0	Z0
	Z0	Z0	Z0	Z0	Z0

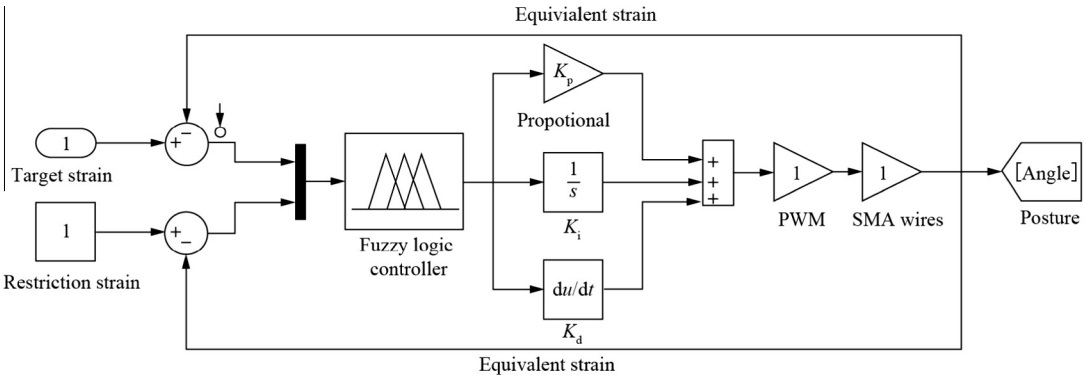

Fig. 12 PID control with a fuzzy supervisor.

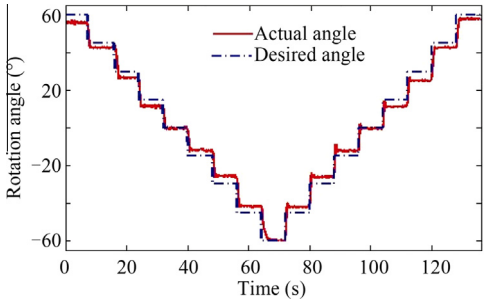

Fig. 13 Multistep response of rotation angles around X and Y directions (desired angle and actual angle).

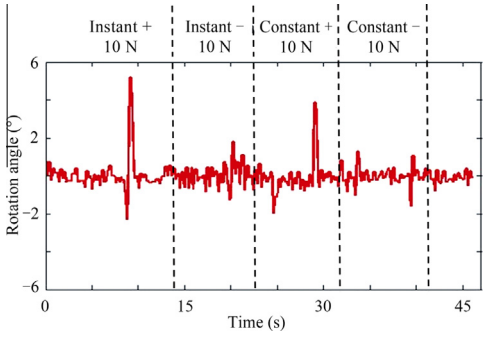

Fig. 14 Disturbance tests to determine control accuracy under external interference.

experiments, as shown in Fig. 14, which presents the camera's measurements. When extra force was applied on the disc, the disturbing internal force changed from +8 N to −8 N, and the force direction was perpendicular to the edge of the disc.

The results showed that with both instantaneous and constant disturbance under 10 N, the strain of the SMA wires had a maximum 5° strain wave, and the overshoot made an opposite wave of strain occur after the disturbance was removed. All interference was eliminated in 1 s with resistance feedback. Note that the ability to resist interference depends on the diameter of the wire, which is limited by the surmounted internal force range.

5. Conclusions

This study presented a two-DOF joint actuated by antagonistic SMA triple wires, which were controlled by a fuzzy PID controller with self-sensing. The instrument's shape and the SMA actuator were designed to achieve a large output in a

limited space. Tests were performed on a trilateral symmetric platform with a three-load cell, and a binocular camera was used to monitor the strain of the SMA wires. A rotational homogeneous transformation matrix was constructed using 12 V, and the *S–R* curves of the three wires were obtained. To minimize the hysteresis gap between the heating and cooling paths of the *S–R* curve, appropriate pre-strain was applied to the triple-wire actuator. In the test of the *S–R* curve under visual control, a wider hysteresis gap appeared near the zero position, due to overstress. Furthermore, a lower heating speed and a fuzzy logic control strategy were considered as solutions. Then, a self-sensing model was constructed by fitting the major loop to three polynomial functions for every wire.

To achieve faster response and avoid overstress simultaneously, a fuzzy PID controller was constructed. The controller included two inputs (the position error e, and the restriction error f) and three outputs (proportional gain K_p, integral gain K_i, and derivative gain K_d). Step-response control experiments showed that the MAE of the rotation angle was 3.147°.

To apply the actuator in practice, further analysis of the external force interference to the system was performed. The result proved that the interference, within a certain range, could be eliminated by resistance feedback control, which determined the controllable maximum output of the actuator. It is expected that the proposed work will be applied to aerospace vehicles and aircraft related robotic arm designs or other driving systems.

Acknowledgements

This study was co-supported by the National Natural Science Foundation of China (61175104) and National Science and Technology Support Program of China (2012BA114B01).

References

1. Otsuka K, Clarence MW. *Shape memory materials*. Cambridge: Cambridge University Press; 1999. p. 10–2.
2. Du SY, Zhan BM. Research on intelligent vehicle structure and its development trend. *J Astronaut* 2007;**28**(4):773–8 [Chinese].
3. Yan XJ, Zhang XY, Nie JX, Zhang SW. Prototype SMA actuated locking device for small space magnetic bearing flywheels. *J Beijing Univ Aeronaut Astronaut* 2011;**37**(2):127–31 [Chinese].
4. Pagedas AC, Inventor, BC, Mabe JH, Calkins FT, Bushnell GS, Bieniawski SR. *Aircraft systems with shape memory alloy (SMA) actuators, and associated methods*. United States patent US 20090212158. 2009.
5. Ming MH, Schetky LM. Industry applications for shape memory alloys. In: *Proceedings of the international conference on shape memory and superelastic technologies*; 2000; Pacific Grove, CA; 2000. p. 171–82.
6. Carballo M, Pu ZJ, Wu KH. Variation of electrical resistance and the elastic modulus of shape memory alloys under different loading and temperature conditions. *J Intell Mater Syst Struct* 1995;**6**(4):557–65.
7. Zhang C, Su J. TiNi shape memory alloy. *Shape Mem Mater* 2003; (2):36–40 [Chinese].
8. Ma N, Song G, Lee HJ. Position control of shape memory alloy actuators with internal electrical resistance feedback using neural networks. *Smart Mater Struct* 2004;**13**(4):777.
9. Lan CC, Fan CH. An accurate self-sensing method for the control of shape memory alloy actuated flexures. *Sens Actuators A: Phys* 2010;**163**(1):323–32.
10. Malukhin K, Ehmann KF. An experimental investigation of the feasibility of self-sensing shape memory alloy based actuators. *J Manuf Sci Eng* 2008;**130**(3):031109.
11. Liu SH, Huang TS, Yen JY. Tracking control of shape-memory-alloy actuators based on self-sensing feedback and inverse hysteresis compensation. *Sensors* 2009;**10**(1):112–27.
12. Takeda Y, Cho H, Yamamoto T, Sakuma T, Suzuki A. Control characteristics of shape memory alloy actuator using resistance feedback control method. *Adv Sci Technol* 2009;**59**:178–83.
13. Urata J, Yoshikai T, Mizuuchi I, Inaba M. Design of high DOF mobile micro robot using electrical resistance control of shape memory alloy. In: *IEEE/RSJ international conference on intelligent robots and systems*; 2007 Oct 29 – Nov 2; California, USA; 2007. p. 3828–33.
14. Teh YH, Featherstone R. An architecture for fast and accurate control of shape memory alloy actuators. *Int J Rob Res* 2008;**27**(5):595–611.
15. Kohl M, Just E, Pfleging W, Miyazaki S. SMA microgripper with integrated antagonism. *Sens Actuators A: Phys* 2000;**83**(1):208–13.
16. Wang Z, Hang G, Li J, Wang Y, Xiao K. A micro-robot fish with embedded SMA wire actuated flexible biomimetic fin. *Sens Actuators A: Phys* 2008;**144**(2):354–60.
17. Bundhoo V, Haslam E, Birch B, Park EJ. A shape memory alloy-based tendon-driven actuation system for biomimetic artificial fingers, Part I: design and evaluation. *Robotica* 2009;**27**(1):131–46.
18. Majima S, Kodama K, Hasegawa T. Modeling of shape memory alloy actuator and tracking control system with the model. *IEEE Trans Control Syst Technol* 2001;**9**(1):54–9.
19. Ge P, Jouaneh M. Tracking control of a piezoceramic actuator. *IEEE Trans Control Syst Technol* 1996;**4**(3):209–16.
20. Raparelli T, Zobel PB, Durante F. SMA wire position control with electrical resistance feedback. In: *Proceedings of the 3rd world conference on structural control*; 2002 Apr 7–11; Como, Italy; 2002. p. 391–8.
21. Song G, Ma N. Control of shape memory alloy actuators using pulse-width pulse-frequency (PWPF) modulation. *J Intell Mater Syst Struct* 2003;**14**(1):15–22.
22. Ma N, Song G. Control of shape memory alloy actuator using pulse width modulation. *Smart Mater Struct* 2003;**12**(5):712–9.
23. Shameli E, Alasty A, Salaarieh H. Stability analysis and nonlinear control of a miniature shape memory alloy actuator for precise applications. *Mechatronics* 2005;**15**(4):471–86.
24. Wang TM, Shi ZY, Liu D, Ma C, Zhang ZH. An accurately controlled antagonistic shape memory alloy actuator with self-sensing. *Sensors* 2012;**12**(6):7682–700.
25. MacNeill D, Freiberger P. *Fuzzy logic*. New York: Simon & Schuster; 1993. p. 160–74.
26. Li H. *Fuzzy logic and intelligent systems*. Massachusetts: Kluwer Academic Pub; 1995. p. 285–302.

Shi Zhenyun is a Ph.D. student in the Robotic Laboratory at Beihang University. He received his M.S. degree from Queen Marry of London University in 2005. His area of research includes control systems, smart actuators, and surgical robots.

Liu Da is a professor and Ph.D. advisor in the Robotic Laboratory at Beihang University, where she received her Ph.D. degree in 2003. Her current research interests are surgical robot technical and computer-assisted intra-operative navigation.